Spin Hall Nano-Oscillator Based on an Antiferromagnetic Domain Wall

R.V. Ovcharov,[1] E.G. Galkina,[2] B.A. Ivanov,[3] and R.S. Khymyn[1,*]

[1] *Department of Physics, University of Gothenburg, Gothenburg 41296, Sweden*

[2] *Institute of Physics, National Academy of Science of Ukraine, Kyiv 03142, Ukraine*

[3] *Institute of Magnetism of the National Academy of Sciences of Ukraine and the Ministry of Education and Science of Ukraine, Kyiv 03142, Ukraine*

(Received 23 July 2021; revised 7 December 2021; accepted 23 June 2022; published 17 August 2022)

We propose here a high-frequency spin-Hall nano-oscillator based on a simple magnetic texture, such as a domain wall, located in an antiferromagnet with an easy-axis anisotropy type. We show that the spin current, polarized along the anisotropy axis, excites a conical precession of the Néel vector in such a domain wall, which allows obtaining a robust ac output signal—contrary to the planar precession in a uniform uniaxial antiferromagnet, where ac output is hard to achieve. The frequency of the auto-oscillations is easily tunable by the applied current up to the terahertz range, and the threshold current vanishes for a pure uniaxial antiferromagnet. By micromagnetic simulations, we demonstrate that the pinning of the domain wall is crucial for the oscillator design, which can be achieved in the nanoconstriction layout of the free layer.

DOI: 10.1103/PhysRevApplied.18.024047

I. INTRODUCTION

Spin-transfer-torque and spin-Hall nano-oscillators (STNOs and SHNOs) are well-established devices in modern spintronics [1–4]. They can act as tiny frequency generators, or as strongly nonlinear "active" elements for advanced signal processing, including neuromorphic [5] and stochastic [6] computing. Both types of oscillators consists of a "free" magnetic layer and an adjunct spin-current source. Spin torque, which arises from the input spin current, drives the magnetization dynamics, which can then be readout as an output electric alternate current. The operational frequency of ferromagnetic devices is defined by the resonant modes of the magnetic layer, i.e., is determined by the bias magnetic field [7,8] and usually lies in the 1–50 GHz range [9], but in practice rarely exceeds 30 GHz.

A significant growth of the operating frequencies, even in the absence of an external field, can be realized in portable spintronics devices by employing antiferromagnetic (AFM) [10,11] or compensated ferrimagnetic [12,13] materials for "free" layers, where a strong exchange field has a definitive contribution to the spin dynamics [14–16]. Thus, the so-called exchange enhancement is applied to the main AFM dynamic parameters: it leads to the ultrahigh frequencies of the magnetic resonance [17], which can reach a terahertz frequency range (0.3–3.0 THz) and substantially high limiting velocity of domain-wall motion [18]. Exchange enhancement also occurs for nonconservative phenomena, such as magnetic damping and spin-transfer torque. Besides, the AFMs can conduct [19], rectify [20], and even amplify [19,21] the spin current.

In the recently proposed AFM-based SHNOs the spin current, polarized along $\mathbf{p}$, induces a torque on the Néel vector $\mathbf{l}$, which starts to rotate in the plane perpendicular to $\mathbf{p}$ [10,11,16,22]. The dynamics of the Néel vector, in turn, can induce an output electric current

$$\mathbf{j}_{\text{out}} \propto \tau_{\text{out}} = [\mathbf{l} \times \dot{\mathbf{l}}] \tag{1}$$

by spin-pumping and inverse spin-Hall mechanisms. Since, for a planar rotation, $\dot{\mathbf{l}} \perp \mathbf{l} \perp \mathbf{p}$ (known as proliferation [10]), the alternate output is present only for the nonuniform in time Néel vector dynamics. This method is applicable to the biaxial AFM with the easy-plane type of primary magnetic anisotropy [11,15], where the in-plane potential created by the small secondary anisotropy accelerates and decelerates the rotation of the Néel vector. This potential, however, creates a threshold for auto-oscillations that would require the application of extremely high currents for its overcoming in the case of easy-axis AFMs. Besides, the above method produces a substantial ac output only not far above the threshold that limits a useful frequency range.

*roman.khymyn@physics.gu.se

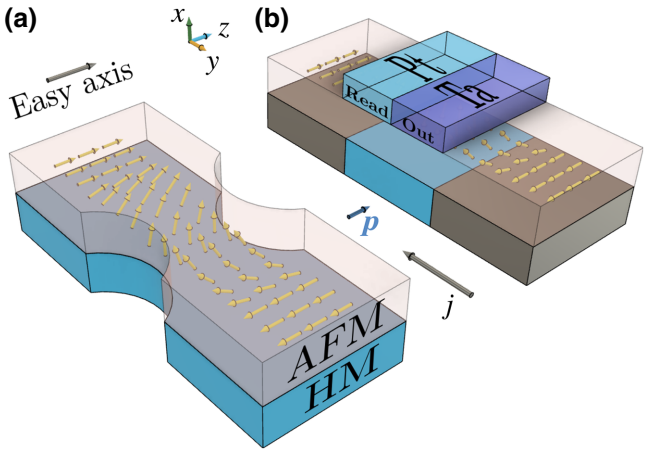

FIG. 1. Schematic diagrams illustrating a microwave generator with a thin film of a uniaxial AFM with domain wall used as an active element in (a) nanoconstriction and (b) rectangular geometries. The Néel vector is shown by the yellow arrows, the black arrow shows the electrical current direction, and the blue arrow indicates the direction of the spin current polarization.

Another way to get the ac signal is to excite the conical precession of **l** for easy-axis AFM [10], or for AFMs in the so-called cone phase [15]. To achieve this, here we propose to use the natural heterogeneity of magnetic order inside magnetic solitons; various types of those already play a significant role in ferromagnetic-based spintronics [23–29]. We consider the simplest topologically stable (the topological charge π_0) soliton, describing a 180° domain wall [30] (DW) and show that nano-oscillators based on an AFM DW can create a substantial ac output while keeping the benefits of the AFM materials, such as ultrahigh achievable frequency. We are focused on the spin-Hall geometry of the device (see Fig. 1); however, the developed theory of the DW dynamics is also applicable for STNOs with 90° rotation of the appropriate axes.

II. SPIN CURRENT DRIVEN DYNAMICS OF A DW

AFM DW motion under the action of spin-orbit torques has already aroused considerable interest in the literature [31,32]. In particular, it was shown that both nonconservative (dampinglike) and conservative (fieldlike) torques can drive the translational motion of the DW with ultrahigh velocities [33–35], which are 2 orders of magnitude higher than those in ferromagnets. Here we are focused on the dynamics of the DW in the easy-axis AFM excited by the dampinglike torque.

For our scheme, the possibility of controlling DWs in a thin film of AFM is of crucial importance. The presence of a weak noncompensated magnetic moment makes the solution simple for easy-axial canted AFM-like orthoferrites. For $DyFeO_3$, canted (weak ferromagnetic) phase is present above the so-called Morin point, approximately 50 K. Thanks to this magnetic moment, a quite-regular domain structure is well known for canted AFMs (see, e.g., Fig. 6 in the review article [36]). An application of nonuniform in space and weak enough magnetic field with the field gradient as small as 0.1 T/cm stabilizes the two-domain configuration with a single DW placed on the line of zero field (see Fig. 10 of Ref. [36]). Even for "pure" AFMs, in particular, for the antiferromagnetic phase of $DyFeO_3$ below the Morin point, DWs were observed optically and controlled by the usage of a combination of a magnetic field and stress [37]. The aforementioned results correspond to films with a thickness of the order of microns, but domain structures are known even for ultrathin magnetic films, and even for magnetic monolayers [38]. Epitaxial films of dysprosium orthoferrite with thicknesses down to 5–10 nm were grown using pulsed laser deposition [39]. For these films, the magnetic structure, including the value of the weak magnetic moment of the order of 0.05 μ_B on an iron ion, is the same as for the bulk material.

The low-energy (in comparison with the energy of the exchange interaction) spin excitation of an AFM can be described by a σ-model equation with a single variable—unit Néel vector **l** [12,16] (normalized by the saturated AFM magnetization value M_s, which corresponds to the parallel orientation of both sublattices). The vector **l** is convenient to represent in angular variables:

$$l_x = \sin\theta\cos\phi, \qquad l_y = \sin\theta\sin\phi, \qquad l_z = \cos\theta. \tag{2}$$

Here the axis z is chosen along the easy axis of the AFM, so that the ground state corresponds to $\theta = 0, \pi$. The Lagrangian density is then [22,40]

$$\mathcal{L} = \frac{M_s}{2\gamma\omega_{\rm ex}}[\dot\theta^2 - c^2\theta'^2 + \sin^2\theta(\dot\phi^2 - c^2\phi'^2)] - w_a, \tag{3}$$

where an upper dot and prime denote derivatives over time and space, respectively, γ is a gyromagnetic ratio, $\omega_{\rm ex} = \gamma H_{\rm ex}$ is the frequency defined by the uniform exchange field $H_{\rm ex}$ of the AFM, and $c = x_0\omega_0 = \gamma\sqrt{H_{\rm ex}A/M_s}$ is the characteristic speed of magnons, which can be written through the domain-wall thickness $x_0 = \sqrt{A/K}$ and the magnon gap $\omega_0 = \gamma\sqrt{H_{\rm ex}K/M_s}$, where A is the inhomogeneous exchange constant. The energy density of the anisotropy reads

$$w_a = \frac{M_s}{2\gamma\omega_{\rm ex}}(\omega_0^2 + \omega_{\rm ip}^2\sin^2\phi)\sin^2\theta, \tag{4}$$

where the first term defines purely uniaxial anisotropy K of the easy-axis type, and the second term defines anisotropy $K_{\rm ip}$ in the basal plane for an AFM with an easy axis of the second order C_2. We are using a finite value of $K_{\rm ip}$ to compare pure uniaxial and nonuniaxial cases.

The natural dissipation and the influx of energy by spin transfer torque (STT) can be expressed in terms of the Rayleigh dissipation function as [15,22]

$$\mathcal{R} = \frac{\alpha M_s}{2\gamma}(\dot{\theta}^2 + \dot{\phi}^2 \sin^2\theta) + \frac{\tau M_s}{\gamma}[p_x(\dot{\theta}\sin\phi + \dot{\phi}\cos\phi\sin 2\theta) - p_z\dot{\phi}\sin^2\theta], \quad (5)$$

where α is an effective Gilbert damping, $\mathbf{p}$ is the unit vector along with spin current polarization, and τ is the amplitude of the STT, expressed in the units of frequency $\tau = \sigma j$ with j the density of the electrical current and σ the STT efficiency [3,41].

The rotation of vector $\mathbf{l}$ in the AFM driven by the spin pumping mechanism generates an output spin current [Eq. (1)] into the adjunct layer with [11,13,15]

$$\tau_{\text{out}} = \omega[\mathbb{z}\sin^2\theta - \sin\theta\cos\theta(\mathbb{x}\cos\omega t + \mathbb{y}\sin\omega t)]. \quad (6)$$

From Eq. (6), the condition $\sin\theta\cos\theta \neq 0$ is required to obtain the ac output. However, in the case of uniform spin dynamics, the angle of stationary precession is determined from the condition $dw_a/d\theta = 0$. From Eq. (4), $dw_a/d\theta \propto \sin\theta\cos\theta$, which corresponds to $\theta = \pi/2$, i.e., the ac signal is absent. Contrary, an ac output appears in the nonuniform state of the Néel order parameter, or spin texture, in the region where $\theta \neq \pi/2$. The simplest example of such a spin texture is a dynamical domain wall with the known profile [42–44]

$$\cos\theta = \tanh\left(\frac{x - X(t)}{\Delta}\right), \qquad \phi = \Phi(t), \quad (7)$$

where Δ is an instant value of the DW thickness; $\Delta = x_0$ for the stationary DW. Using the solution of the DW profile (7) and assuming that $\alpha \ll 1$ and $\tau \ll \omega_0$, we can write down the equations of motion through the collective coordinates: the coordinate of the wall center X and the angle Φ, which determines the rotation angle of vector $\mathbf{l}$ in the wall center (see the Supplemental Material [45]). We have

$$\frac{1}{\omega_{\text{ex}}}\frac{d}{dt}\left(\frac{\dot{X}}{\Delta}\right) + \alpha\frac{\dot{X}}{\Delta} + \tau\frac{\pi}{2}(p_x\sin\Phi - p_y\cos\Phi) = 0, \quad (8)$$

$$\frac{1}{\omega_{\text{ex}}}\frac{d}{dt}(\Delta\dot{\Phi}) + \alpha\Delta\dot{\Phi} - \Delta\tau p_z + \Delta\frac{\omega_{\text{ip}}^2}{2\omega_{\text{ex}}}\sin 2\Phi = 0, \quad (9)$$

where $\Delta = x_0\sqrt{1 - \dot{X}^2/c^2}\Big/\sqrt{1 - \dot{\Phi}^2/\omega_0^2}$.

Equations (8) and (9) form one of the main analytical results of this work: they show the possibility of excitation of both the rotational ($p_z \neq 0$) and translational ($p_x, p_y \neq 0$) dynamics of the domain wall by the spin current. With this in mind, below, we discuss in detail the possibility of creating a spin-torque nanogenerator based on the AFM domain wall and analyze the regimes of its operation depending on the polarization direction of the spin current.

III. MICROMAGNETIC SIMULATIONS

To verify analytical results, we perform micromagnetic simulations using the MUMAX^3 solver [46] employing method similar to that described in Refs. [47,48]. We choose two geometries of the SHNO: the rectangular geometry, which completely represents our analytical model, and the nanoconstriction (NC; see Fig. 1) geometry. The NC cutout not only increases the local current density but also induces a pinning potential for the DW since the minimal length and accordingly the minimal energy of the DW is reached at the center of the NC. Therefore, in a pure AFM without another induced pinning center, a DW created anywhere within a NC area will naturally relax into the center position, which makes this geometry advantageous for practical applications. As an AFM layer, we choose dysprosium orthoferrite $DyFeO_3$, in which the anisotropy in the easy plane changes its sign at temperature $T = 150$ K, and hence can be chosen arbitrarily weak (this property has been established by investigation of the DW structure [49], magnetic resonance measurements [50], and the pump-probe technique [51]). As a spin-Hall layer, Pt is chosen. Thus, we choose the following parameters [17,52]: $\theta_{\text{SH}} = 0.1$, $\alpha = 10^{-3}$, $M_s = 8.4 \times 10^5$ A/m, $A = 18.9$ pJ/m, $H_{\text{ex}} = 670$ T, the anisotropy constant along the easy axis $K = 300$ kJ/m^3, the value of the weak secondary AFM anisotropy $K_{\text{ip}} = 2$ kJ/m^3. Simulations are performed for the 136-nm-wide sample (for both cases) with a centrally located NC with a width of 100 nm and a cutout radius of 50 nm. For the rectangular shape, the length of the Pt layer is limited to $L = 100$ nm to study the stability of the DW position.

IV. RESULTS AND COMPARISON WITH THE THEORY

For further analysis of the DW dynamics, we introduce the angle ψ, which determines the direction of the polarization vector $\mathbf{p} = \mathbb{z}\cos\psi + \mathbb{y}\sin\psi$. The angle ψ is easily configurable in STNOs, where the adjunct layer determines the polarization of the spin current. However, in SHNOs $\mathbf{p}$ is strictly determined by the direction of the electrical current, and in the chosen configuration corresponds to the z direction. Thus, the direction of the easy axis should be changed to obtain a nonzero angle ψ. In this case, the domain wall itself does not change its position, as it is not bound to the spin frame of reference, but the direction of the output torque is changed; see details below. For this case, we introduce another angle φ_{DW} that determines

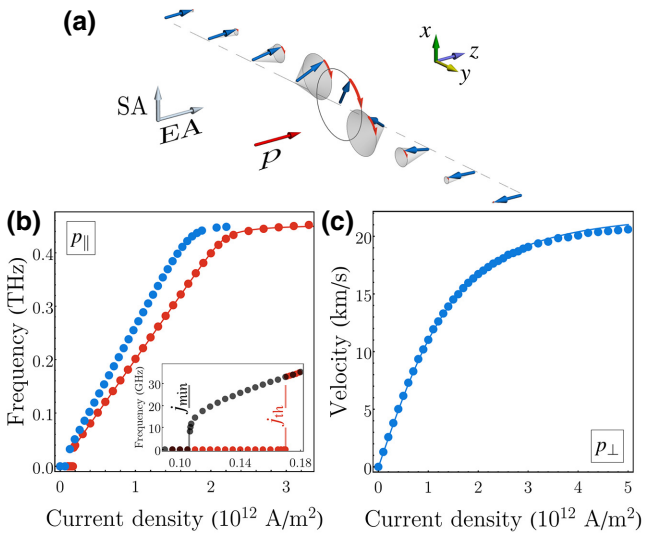

FIG. 2. (a) Sketch of a Néel vector precession within a DW under the action of direct spin current. Gray arrows show the directions of the easy axis (EA) and secondary anisotropy (SA). (b) Frequency $\omega/2\pi$ of the DW rotation for the NC (blue) and rectangular (red) geometries. (c) Velocity of the DW as a function of the dc electric current density. Dots show the values extracted from the micromagnetic simulations, while solid lines are calculated analytically. The frequency of the AFM resonance $\omega_0/2\pi = 0.45$ THz and the limiting velocity $c = 22$ km/s.

the deviation of the easy axis relative to the DW orientation (z axis).

Parallel polarization: $\mathbf{p} = \mathbb{z}$, $\psi = 0°$. The solution for the DW coordinate X corresponds to the standing wall, as $p_x = p_y = 0$ in Eq. (8). From Eq. (9) it follows that the spin current, with polarization along the easy axis p_z, excites Josephson-like dynamics [11] that leads to the rotation of the Néel vector within a DW under the action of direct spin current, as is schematically shown in Fig. 2(a). The precession of the Néel vector is of a conical type, similar to the precession of magnetization in ferromagnetic oscillators. However, in ferromagnetic counterparts, the cone opening angle is defined by a balance between applied torque and nonlinear damping. In contrast, here it is determined by a spatial position within a DW, according to the Eq. (7) and is independent on torque and damping in a wide frequency range, when $\dot{\Phi} \ll \omega_0$ is negligible in the expression for a DW thickness Δ.

Josephson-like spin dynamics, described by Eq. (9), has been widely discussed in the literature in the application to uniform easy-plane AFM materials [11,53]. Equation (9) is mathematically analogous to the dynamics of a physical pendulum in a gravitational potential under the action of constant external torque. In this analogy, the magnetic anisotropy ω_{ip} plays the role of a gravitational field, and Gilbert damping plays the role of friction. Therefore, the threshold torque (i.e., current) to start auto-oscillations (rotation of the pendulum) is defined only by the potential energy at the "top" position, i.e., by the anisotropy value as $\sigma j_{th} = \omega_{ip}^2/(2\omega_{ex})$ and does not depend on damping. The value of j_{th}, which is relatively small for our parameters, vanishes for pure uniaxial AFM, and an arbitrarily weak current excites spin dynamics with a low frequency.

In the case of a limited spin-current source size with length L, at currents above the threshold, the dependence of the frequency on the current is determined by a balance between the total energy loss in the whole DW and energy gain within the limited spin-current contact area. By integrating the energy balance function with corresponding limits (see the Supplemental Material [45]), one can obtain

$$\alpha\omega = \sigma j \tanh\left(\frac{L}{2x_0}\sqrt{1-\frac{\omega^2}{\omega_0^2}}\right). \tag{10}$$

In the case of a large spin-torque source, $L \gg x_0$ and $\omega \ll \omega_0$, the frequency of the rotation is linearly proportional to the driving current $\omega = \sigma j/\alpha$. The minimum frequency achievable by a constant torque can be obtained by substituting the threshold and reads $\omega_{th} \simeq \sigma j_{th}/\alpha = \omega_{ip}^2/(2\alpha\omega_{ex})$. Thus, Eq. (10) implies easy tunability of the frequency by the driving current in the range ω_{th}–ω_0, where ω_0 can reach a subterahertz range. The numerical simulation of such a regime is represented in Fig. 2(b) by symbols, while the solution of Eq. (10) for a rectangular sample is shown by a solid red line. The rapid saturation of the generation frequency when approaching the AFM resonance ω_0 is caused by an expansion of the DW thickness Δ and, hence, by a reduction of a relative overlap with a spin current source.

The first term of Eq. (9), which is inversely proportional to the exchange frequency, also implies an inertial dynamics of the oscillator. Once started, a Néel vector will continue to precess even with torques below the aforementioned threshold in the case of a low damping value, which we assume here. To stop oscillations, the losses have to overcome the energy gain over the cycle, which gives the minimum current $\sigma j_{min} \simeq 2\alpha\omega_{ip}/\pi$ of sustained oscillations [11], as shown in the inset of Fig. 2(b). To simulate this regime, a short (0.5 ns) rectangular pulse of a current above the threshold ($j > j_{th}$) is applied to start spin dynamics, which is later reduced to the desired values of $j < j_{th}$[11]. In this way, one can reach arbitrarily low frequencies of the oscillations near j_{min}, but has to take into account a large amplitude of high harmonics [53].

Given Eq. (6) for this case, one can note that the output alternate spin current is spatially asymmetric:

$$\tau_{out}^y = \omega \mathrm{sech}\left(\frac{x}{\Delta}\right)\tanh\left(\frac{x}{\Delta}\right)\cos\omega t. \tag{11}$$

Since $\mathbf{I}_{out} \propto \int \tau_{out} dxdy$ averaged over the DW vanishes, see Figs. 3(a) and 3(b), the signals from the film areas,

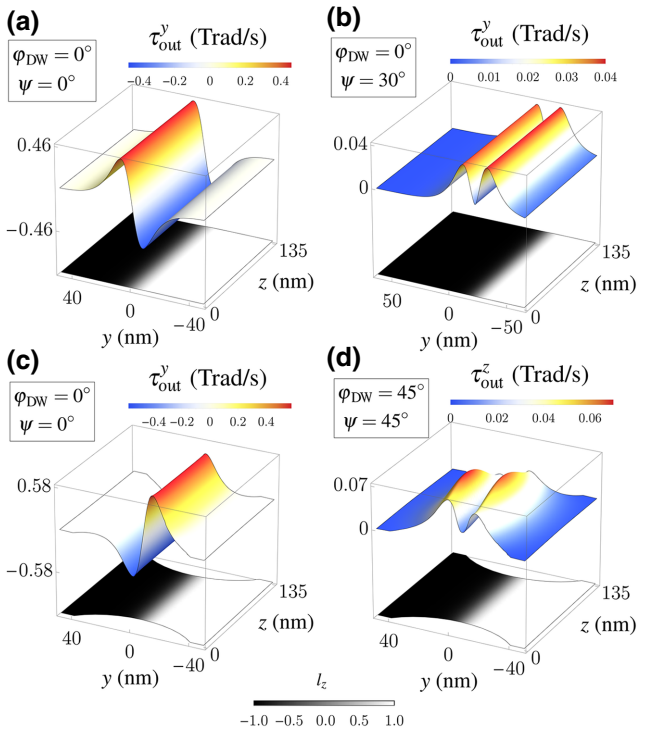

FIG. 3. Simulated distributions of the output torque $\tau_{out} = \mathbf{l} \times \partial\mathbf{l}/\partial t$ components (the upper plane in each figure) and z component of the Néel vector (the lower one) in the plane of the film for different geometries [rectangular (a),(b) and NC (c),(d)] and different spin polarization angles [$\psi = 0°$ (a),(c), $\psi = 30°$ (b) and $\psi = 45°$ (d)]. The applied current density is 7.8×10^{11} A/m^2. Panels (a) and (c) show alternate torque at the primary frequency of oscillations $\omega/2\pi = 160$ GHz [Eq. (11)], while panels (b) and (d) show alternate torque at the doubled frequency $2\omega/2\pi = 320$ GHz [Eq. (16)].

where $\sin\theta\cos\theta \lessgtr 0$ have to be read out independently, can be achieved by an additional spin-Hall electrode on top of the AFM layer. As well, a unique technique used in Ref. [54] can be applied, where two nanowires made of metals with opposite signs for the spin-Hall angle (such as, e.g., tantalum and platinum) are placed at opposite slopes of the DW to sum up the signals [see Fig. 1(b)].

Perpendicular polarization: $\mathbf{p} = \mathbb{y}$, $\psi = 90°$. In this limit case, the precessional dynamics is not excited, and only the translational motion of the DW is possible, which was already highlighted in the literature [31,33,55]. The equation for the velocity of DW motion is common to that for a DW driven by Néel spin-orbit torques, considered in detail in Ref. [34] (see also the Supplemental Material [45] for details), namely,

$$v = \mu\tau c/\sqrt{(\mu\tau)^2 + c^2}, \tag{12}$$

where $\mu = \pi x_0/2\alpha$ has the sense of the mobility of the domain wall ($v \simeq \mu\tau$ at $\mu\tau \ll c$). The dependence of the velocity on the applied current for the rectangular geometry is shown in Fig. 2(c).

Oblique polarization: $0° < \psi < 90°$. In this case, the torque component (p_z) defines the solution for the angle Φ in Eq. (9) and, thus, controls the efficiency of the driving force in Eq. (8). As in the case of $\psi = 0$, the anisotropy in the hard plane induces the threshold for the oscillations. Above the threshold $j \gg j_{th}$, particularly for pure uniaxial AFM, when $j_{th} = 0$, the solution takes the form $\Phi \approx \omega t$ that leads to oscillations of the domain wall around the equilibrium position with the velocity defined by

$$\frac{\dot{X}}{\sqrt{1 - \dot{X}^2/c^2}} = \Delta(\omega)\frac{\pi p_y}{2}\frac{\tau\omega_{ex}}{\sqrt{\omega^2 + \alpha^2\omega_{ex}^2}}\sin(\omega t + \varphi), \tag{13}$$

where $\Delta(\omega) = x_0/\sqrt{1 - \omega^2/\omega_0^2}$ and $\varphi = \arctan(\alpha\omega_{ex}/\omega)$.

Taking, for simplicity, $\dot{X} \ll c$, the coordinate can be written as

$$X(t) = X_{max}\cos(\omega t + \varphi), \tag{14}$$

where the amplitude of the DW translational oscillations is defined by

$$X_{max} = \frac{\pi p_y}{2p_z}\frac{\alpha\omega_{ex}}{\sqrt{\omega^2 + \alpha^2\omega_{ex}^2}}\Delta(\omega). \tag{15}$$

However, the analytical solution $\Phi = \omega t$ is approximate [11], and our micromagnetic simulations show that periodic wall oscillations are accompanied by a drift; see Fig. 4(a). This drift is a significant problem for the signal readout in a rectangular geometry; depending on the polarization of the spin current, angle Φ, and velocity of the domain wall, it can bounce off the edge of the contact, stay on the edge for a long time, or go beyond the STT source area, which will disrupt signal generation [see Fig. 4(a) for $\psi = 45°$]. This problem can be solved by pinning the wall, such as using NC; see Fig. 4(b). The NC creates a restoring force for the DW, so, as can be seen from the simulations, the wall ceases to drift, and the points of the phase change are fixed in coordinate. Interestingly, the amplitude of the oscillations increases as the DW exhibits resonant behavior in the pinning potential.

The translational oscillations of the DW produce an additional output torque at the doubled frequency:

$$\tau^y_{out} = \frac{\omega X_{max}}{\Delta}\,\mathrm{sech}\left(\frac{x - X(t)}{\Delta}\right)\cos 2\omega t. \tag{16}$$

In contrast to Eq. (11), the signal is symmetrical in coordinate [see Figs. 3(c) and 3(d)], so there is no need for the additional readout layers. However, τ^y_{out} creates an electrical current in the z direction, i.e., perpendicular to the

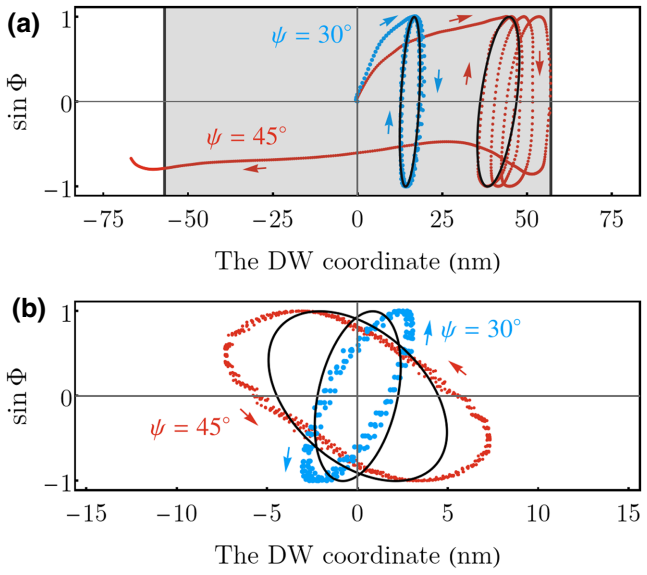

FIG. 4. The phase of the domain wall Φ as a function of the domain-wall coordinate X for the (a) rectangular and (b) NC geometries. The gray rectangle defines the spin-Hall region, where current is flowing; black ellipses show analytical dependence (14). The applied current density is 2.4×10^{11} A/m^2.

input one, which requires a complex four-terminal device design. To avoid this issue, one can tilt the easy axis of the AFM in the y-z plane by an angle φ_{DW}, and as a result, an alternating z component appears in the output torque. In this case, the same two terminals can be used simultaneously as a source of the dc input and a detector of the ac output as in conventional spin-Hall oscillators.

The output power of the SHNO can be calculated using the method described in Ref. [11]. It is presented in Fig. 5 for the aforementioned parameters of the SHNO. The useful signal at frequency ω of the DW precession achieves higher power, although it requires additional readout layers. However, even at the doubled frequency

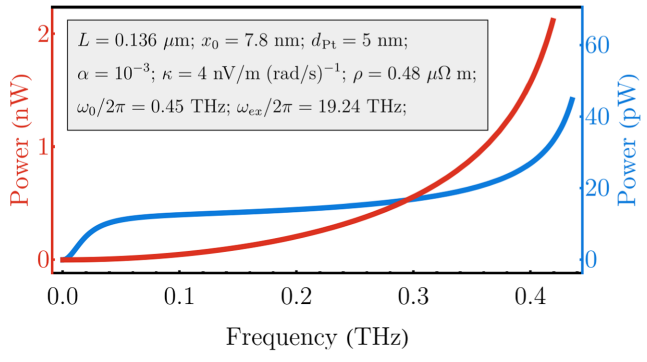

FIG. 5. The output power of the spin-Hall nano-oscillator. The red line corresponds to $\psi = 0°, \phi_{\mathrm{DW}} = 0°$ and is extracted at the main frequency of oscillations ω, while the blue line is extracted at the doubled 2ω and $\psi = 45°, \phi_{\mathrm{DW}} = 45°$.

2ω and simple bilayer SHNO layout, the output power can reach tens of picowatts for 100-nm DW length, which is a few times higher than for the conventional ferromagnetic devices [24]. It is noticeable that power delivered by both output methods substantially grows near the AFM resonance frequency ω_0, which makes it preferable to operate in the high-frequency range.

V. CONCLUSIONS

To conclude, first note that the developed theory is not limited to AFM dielectrics and is also applicable to metallic AFM films. Usually, however, AFM metals have a substantially higher damping α, which leads to the lower slope of the oscillation frequency versus current (Fig. 2) for the same STT efficiency σ. Besides, in this case, an oscillator has only one threshold j_{th}, since $j_{\mathrm{min}} > j_{\mathrm{th}}$, and oscillations start from zero frequency with multiple harmonics in the spectrum (see the details in Ref. [53]).

Thus, we have shown that the spin current can excite complex dynamical regimes for an AFM DW, which include the precession of the Néel vector in the center of a DW, as well as oscillatory motion of the DW position. This dynamics provides a substantial alternate output spin current, which can be used for the development of efficient subterahertz spin-Hall nano-oscillators. The pronounced feature of this oscillator offers the possibility of minimizing a threshold current (which completely vanishes in the case of a pure uniaxial anisotropy) and the increasing of the output power with the frequency; see Fig. 5.

ACKNOWLEDGMENTS

This project is funded by the European Research Council (ERC) under the European Union's Horizon 2020 research and innovation programme (Grant TOPSPIN No 835068). B.A.I. acknowledges support from the National Research Foundation of Ukraine, under Grant No. 2020.02/0261.

[1] V. E. Demidov, S. Urazhdin, H. Ulrichs, V. Tiberkevich, A. Slavin, D. Baither, G. Schmitz, and S. O. Demokritov, Magnetic nano-oscillator driven by pure spin current, Nat. Mater. **11**, 1028 (2012).

[2] V. Demidov, S. Urazhdin, A. Zholud, A. Sadovnikov, and S. Demokritov, Nanoconstriction-based spin-Hall nano-oscillator, Appl. Phys. Lett. **105**, 172410 (2014).

[3] A. Slavin and V. Tiberkevich, Nonlinear auto-oscillator theory of microwave generation by spin-polarized current, IEEE Trans. Magn. **45**, 1875 (2009).

[4] T. Chen, R. K. Dumas, A. Eklund, P. K. Muduli, A. Houshang, A. A. Awad, P. Dürrenfeld, B. G. Malm, A. Rusu, and J. Åkerman, Spin-torque and spin-Hall nano-oscillators, Proc. IEEE **104**, 1919 (2016).

[5] J. Grollier, D. Querlioz, K. Camsari, K. Everschor-Sitte, S. Fukami, and M. D. Stiles, Neuromorphic spintronics, Nat. Electron. **3**, 360 (2020).

[6] N. Locatelli, V. Cros, and J. Grollier, Spin-torque building blocks, Nat. Mater. **13**, 11 (2014).

[7] S. Bonetti, V. Tiberkevich, G. Consolo, G. Finocchio, P. Muduli, F. Mancoff, A. Slavin, and J. Åkerman, Experimental Evidence of Self-Localized and Propagating Spin Wave Modes in Obliquely Magnetized Current-Driven Nanocontacts, Phys. Rev. Lett. **105**, 217204 (2010).

[8] A. Houshang, R. Khymyn, H. Fulara, A. Gangwar, M. Haidar, S. Etesami, R. Ferreira, P. Freitas, M. Dvornik, R. Dumas, and J. Åkerman, Spin transfer torque driven higher-order propagating spin waves in nano-contact magnetic tunnel junctions, Nat. Commun. **9**, 1 (2018).

[9] S. Bonetti, P. Muduli, F. Mancoff, and J. Åkerman, Spin torque oscillator frequency versus magnetic field angle: The prospect of operation beyond 65 GHz, Appl. Phys. Lett. **94**, 102507 (2009).

[10] R. Cheng, D. Xiao, and A. Brataas, Terahertz Antiferromagnetic Spin Hall Nano-Oscillator, Phys. Rev. Lett. **116**, 207603 (2016).

[11] R. Khymyn, I. Lisenkov, V. Tiberkevich, B. A. Ivanov, and A. Slavin, Antiferromagnetic THz-frequency Josephson-like oscillator driven by spin current, Sci. Rep. **7**, 1 (2017).

[12] B. A. Ivanov, Ultrafast spin dynamics and spintronics for ferrimagnets close to the spin compensation point, Low Temp. Phys. **45**, 935 (2019).

[13] I. Lisenkov, R. Khymyn, J. Åkerman, N. X. Sun, and B. A. Ivanov, Subterahertz ferrimagnetic spin-transfer torque oscillator, Phys. Rev. B **100**, 100409 (2019).

[14] V. Baltz, A. Manchon, M. Tsoi, T. Moriyama, T. Ono, and Y. Tserkovnyak, Antiferromagnetic spintronics, Rev. Mod. Phys. **90**, 015005 (2018).

[15] B. A. Ivanov, Spin dynamics for antiferromagnets and ultrafast spintronics, J. Exp. Theor. Phys. **131**, 95 (2020).

[16] E. Gomonay and V. Loktev, Spintronics of antiferromagnetic systems, Low Temp. Phys. **40**, 17 (2014).

[17] E. Turov, A. Kolchanov, M. Kurkin, I. Mirsaev, and V. Nikolaev, *Symmetry and Physical Properties of Antiferromagnets* (Fizmatlit, Moscow, 2001).

[18] V. G. Bar'yakhtar, M. V. Chetkin, B. A. Ivanov, and S. N. Gadetskii, *Dynamics of Topological Magnetic Solitons: Experiment and Theory* (Springer Verlag, Berlin, 1994), Vol. 129.

[19] H. Wang, C. Du, P. C. Hammel, and F. Yang, Antiferromagnonic Spin Transport from $Y_3Fe_5O_{12}$ into NiO, Phys. Rev. Lett. **113**, 097202 (2014).

[20] R. Khymyn, V. Tiberkevich, and A. Slavin, Antiferromagnetic spin current rectifier, AIP Adv. **7**, 055931 (2017).

[21] R. Khymyn, I. Lisenkov, V. S. Tiberkevich, A. N. Slavin, and B. A. Ivanov, Transformation of spin current by antiferromagnetic insulators, Phys. Rev. B **93**, 224421 (2016).

[22] H. V. Gomonay and V. M. Loktev, Spin transfer and current-induced switching in antiferromagnets, Phys. Rev. B **81**, 144427 (2010).

[23] M. Hoefer, T. J. Silva, and M. W. Keller, Theory for a dissipative droplet soliton excited by a spin torque nanocontact, Phys. Rev. B **82**, 054432 (2010).

[24] S. M. Mohseni, S. Sani, J. Persson, T. A. Nguyen, S. Chung, Y. Pogoryelov, P. Muduli, E. Iacocca, A. Eklund, R. Dumas, S. Bonetti, A. Deac, M. A. Hoefer, and J. Åkerman, Spin torque–generated magnetic droplet solitons, Science **339**, 1295 (2013).

[25] Y. Zhou, E. Iacocca, A. A. Awad, R. K. Dumas, F. Zhang, H. B. Braun, and J. Åkerman, Dynamically stabilized magnetic skyrmions, Nat. Commun. **6**, 1 (2015).

[26] E. Iacocca, R. K. Dumas, L. Bookman, M. Mohseni, S. Chung, M. A. Hoefer, and J. Åkerman, Confined Dissipative Droplet Solitons in Spin-Valve Nanowires with Perpendicular Magnetic Anisotropy, Phys. Rev. Lett. **112**, 047201 (2014).

[27] S. Chung, A. Eklund, E. Iacocca, S. M. Mohseni, S. R. Sani, L. Bookman, M. A. Hoefer, R. K. Dumas, and J. Åkerman, Magnetic droplet nucleation boundary in orthogonal spin-torque nano-oscillators, Nat. Commun. **7**, 1 (2016).

[28] S. Chung, Q. T. Le, M. Ahlberg, A. A. Awad, M. Weigand, I. Bykova, R. Khymyn, M. Dvornik, H. Mazraati, and A. Houshang *et al.*, Direct Observation of Zhang-Li Torque Expansion of Magnetic Droplet Solitons, Phys. Rev. Lett. **120**, 217204 (2018).

[29] N. Sato, K. Schultheiss, L. Körber, N. Puwenberg, T. Mühl, A. Awad, S. Arekapudi, O. Hellwig, J. Fassbender, and H. Schultheiss, Domain Wall Based Spin-Hall Nano-Oscillators, Phys. Rev. Lett. **123**, 057204 (2019).

[30] O. Gomonay, V. Baltz, A. Brataas, and Y. Tserkovnyak, Antiferromagnetic spin textures and dynamics, Nat. Phys. **14**, 213 (2018).

[31] K. M. Hals, Y. Tserkovnyak, and A. Brataas, Phenomenology of Current-Induced Dynamics in Antiferromagnets, Phys. Rev. Lett. **106**, 107206 (2011).

[32] R. Cheng and Q. Niu, Dynamics of antiferromagnets driven by spin current, Phys. Rev. B **89**, 081105 (2014).

[33] T. Shiino, S.-H. Oh, P. M. Haney, S.-W. Lee, G. Go, B.-G. Park, and K.-J. Lee, Antiferromagnetic Domain Wall Motion Driven by Spin-Orbit Torques, Phys. Rev. Lett. **117**, 087203 (2016).

[34] O. Gomonay, T. Jungwirth, and J. Sinova, High Antiferromagnetic Domain Wall Velocity Induced by Néel Spin-Orbit Torques, Phys. Rev. Lett. **117**, 017202 (2016).

[35] Z. Li and S. Zhang, Domain-Wall Dynamics and Spin-Wave Excitations with Spin-Transfer Torques, Phys. Rev. Lett. **92**, 207203 (2004).

[36] V. G. Bar'yakhtar, B. A. Ivanov, and M. V. Chetkin, Dynamics of domain walls in weak ferromagnets, Soviet Phys. Uspekhi **28**, 563 (1985).

[37] D. Afanasiev, B. A. Ivanov, A. Kirilyuk, T. Rasing, R. Pisarev, and A. Kimel, Control of the Ultrafast Photoinduced Magnetization Across the Morin Transition in $DyFeO_3$, Phys. Rev. Lett. **116**, 097401 (2016).

[38] E. Y. Vedmedenko, H. Oepen, A. Ghazali, J.-C. Lévy, and J. Kirschner, Magnetic Microstructure of the Spin Reorientation Transition: A Computer Experiment, Phys. Rev. Lett. **84**, 5884 (2000).

[39] T.-Y. Khim, M. Eom, J. Kim, B.-G. Park, J.-Y. Kim, and J.-H. Park, Strain control spin reorientation transition in $DyFeO_3/SrTiO_3$ epitaxial film, Appl. Phys. Lett. **99**, 072501 (2011).

[40] A. M. Kosevich, B. A. Ivanov, and A. S. Kovalev, Magnetic solitons, Phys. Rep. **194**, 117 (1990).
[41] A. Slavin and V. Tiberkevich, Theory of mutual phase locking of spin-torque nanosized oscillators, Phys. Rev. B **74**, 104401 (2006).
[42] S. K. Kim, Y. Tserkovnyak, and O. Tchernyshyov, Propulsion of a domain wall in an antiferromagnet by magnons, Phys. Rev. B **90**, 104406 (2014).
[43] E. G. Galkina, R. Ovcharov, and B. A. Ivanov, Precessional one-dimensional solitons in antiferromagnets with low dynamic symmetry, Low Temp. Phys. **43**, 1283 (2017).
[44] B. A. Ivanov and A. K. Kolezhuk, Solitons with Internal Degrees of Freedom in 1D Heisenberg Antiferromagnets, Phys. Rev. Lett. **74**, 1859 (1995).
[45] See Supplemental Material at http://link.aps.org/supplemental/10.1103/PhysRevApplied.18.024047, which includes Ref. [56], for the description of the collective coordinates approach and details of the micromagnetic simulations.
[46] A. Vansteenkiste, J. Leliaert, M. Dvornik, M. Helsen, F. Garcia-Sanchez, and B. Van Waeyenberge, The design and verification of MuMax3, AIP Adv. **4**, 107133 (2014).
[47] J. De Clercq, J. Leliaert, and B. Van Waeyenberge, Modelling compensated antiferromagnetic interfaces with MuMax^3, J. Phys. D: Appl. Phys. **50**, 425002 (2017).
[48] D. Suess, T. Schrefl, W. Scholz, J.-V. Kim, R. Stamps, and J. Fidler, Micromagnetic simulation of antiferromagnetic/ferromagnetic structures, IEEE Trans. Magn. **38**, 2397 (2002).
[49] A. Zalesskij, A. Savvinov, I. Zheludev, and A. Ivashchenko, NMR of Fe^{57} nuclei and spin reorientation in domains and domain walls of $ErFeO_3$ and $DyFeO_3$ crystals, Zhurnal Ehksperimental'noj i Teoreticheskoj Fiziki **68**, 1449 (1975).
[50] A. Balbashov, A. Volkov, S. Lebedev, A. Mukhin, and A. Prokhorov, High-frequency magnetic properties of dysprosium orthoferrite, Zh. Eksp. Teor. Fiz **88**, 974 (1985).
[51] A. Kimel, A. Kirilyuk, P. Usachev, R. Pisarev, A. Balbashov, and T. Rasing, Ultrafast non-thermal control of magnetization by instantaneous photomagnetic pulses, Nature **435**, 655 (2005).
[52] M.-H. Nguyen, D. Ralph, and R. Buhrman, Spin Torque Study of the Spin Hall Conductivity and Spin Diffusion Length in Platinum Thin Films with Varying Resistivity, Phys. Rev. Lett. **116**, 126601 (2016).
[53] R. Khymyn, I. Lisenkov, J. Voorheis, O. Sulymenko, O. Prokopenko, V. Tiberkevich, J. Akerman, and A. Slavin, Ultra-fast artificial neuron: Generation of picosecond-duration spikes in a current-driven antiferromagnetic auto-oscillator, Sci. Rep. **8**, 1 (2018).
[54] J. Li, C. B. Wilson, R. Cheng, M. Lohmann, M. Kavand, W. Yuan, M. Aldosary, N. Agladze, P. Wei, M. S. Sherwin, and Jing Shi, Spin current from sub-terahertz-generated antiferromagnetic magnons, Nature **578**, 70 (2020).
[55] L. Sánchez-Tejerina, V. Puliafito, P. K. Amiri, M. Carpentieri, and G. Finocchio, Dynamics of domain-wall motion driven by spin-orbit torque in antiferromagnets, Phys. Rev. B **101**, 014433 (2020).
[56] Y. S. Kivshar and B. A. Malomed, Dynamics of solitons in nearly integrable systems, Rev. Mod. Phys. **61**, 763 (1989).